



Experiment on Erosion Wear Characteristic of NiWC35 Coating and Sintered WC under High-Speed Impacting of Solid Particle

C. Wang¹, A. Q. Duan¹, K. N. Bie¹, X. F. Liu¹, H. Z. Jin^{1†} and G. F. Ou²

¹ Faculty of Mechanical Engineering & Automation, Zhejiang Sci-Tech University, Hangzhou, Zhejiang, 310018, China

² School of Mechanical Engineering & Rail Transit, Changzhou University, Changzhou, Jiangsu, 213000, China

†Corresponding Author Email: haozhe2007@163.com

(Received September 8, 2020; accepted December 16, 2020)

ABSTRACT

Erosion wear caused by solid particles is a big challenge in the oil and gas industry, which seriously threatens the long-term safe operation of the equipment. A novel experimental apparatus was set up to meet the requirements for accelerating erosion wear research process for abrasion resistant materials, with a capability of producing high speed particles to impact target specimen. The erosion wear experiments of NiWC35 coating and sintered WC were conducted under different amounts of abrasive, temperatures, and impact angles respectively. Their macroscopic and microscopic erosion damage morphology and mechanism were discussed and analyzed. The results show that the amount of abrasive, temperature and impact angle have a more significant effect on the erosion wear of NiWC35 coating than sintered WC. The erosion rate of NiWC35 coating increases approximately linearly with the increase of the amount of abrasive; the impact angle of the NiWC35 coating is smaller, the range of erosion pit is wider; while the erosion wear morphology and erosion rate of sintered WC basically unchanged under different variables, countless fine irregular particles in the microscopic surface is the key to excellent abrasion resistance of sintered WC.

Keywords: Erosion wear experiment; NiWC35 coating; Sintered WC; Abrasion resistance; Impact morphology.

NOMENCLATURE

E	erosion wear rate	$V\alpha$	impact velocity
m_p	solid particle mass	Δm_t	lost mass
t	experimental time		

1. INTRODUCTION

Coal gasification technology is the mainstream core of coal deep processing, through the reaction of coal water slurry with oxidant and catalyst in gasifier under high temperature and high pressure, combustible gases such as CO, H₂ and CH₄ are generated and used in chemical raw materials, combined power generation, metallurgical reduction gas and other industrial fields (Xiao *et al.* 2020). It is of great significance for clean and efficient utilization of coal resources (Li *et al.* 2019). The high-pressure black water and grey water treatment systems in coal gasification plant contain high concentration of pulverized coal particles, and the

content of particles in some media is even as high as 12% ~ 15% (Zheng *et al.* 2016). In the process of pipeline transportation containing solid particles, the failure of valves and pipelines caused by impact accounts for more than 40% of all failure forms, which seriously affects the stability of transportation process and the safe operation of equipment (Chen *et al.* 2020). Therefore, gas-solid two-phase flow erosion wear caused by solid particles widely exists in coal gasification process, which is a crucial factor restricting the long-term operation of equipment (Ou *et al.* 2019; Ilieva *et al.* 2017). The thinning and leakages of pipes and equipment caused by the particle erosion wear have become the difficult problem in the coal chemical

industry (More *et al.* 2018; Singh *et al.* 2018). NiWC35 coating and sintered WC is widely used to welded to the surface of critical position of coal gasification equipment to extend the life of equipment and pipelines (Bhosale *et al.* 2020). Therefore, it is urgent to carry out the research on the gas-solid two-phase flow erosion properties of NiWC35 coating and sintered WC.

In the previous work, experiment, material properties and mechanism of gas-solid two-phase flow erosion wear had been investigated by many scientists, which is helpful and instructive to the process of research and the design of test (Varga *et al.* 2019). Hu *et al.* (2020) applied the experimental design method to investigate erosion properties of 9Cr-1MoVNb at high temperatures and analyzed the surface damage by scanning electron microscope, erosion mechanism was obtained in the following order: plastic deformation due to the collision of spherical particles followed by cracks due to repetitive fatigue, and separation of debris due to crack growth. Lin *et al.* (2020) designed the gas-solid two-phase flow experiment to study the erosion characteristics of the gate valve and validated the accuracy of the numerical simulation, the results indicate that the number of particles plays an important role in erosion rate. The related materials of protective wear resistant coatings used for the protection of hydro turbine system was introduced by Kumar *et al.* (2018), the resistance to erosive wear of WC based coatings widely used in industry was found to be better. Experiment and numerical simulation were conducted by Kim *et al.* (2015), the erosion rate of hard metal WC-Ni widely used in industries is increased due to the increase of the hardness.

The effects of the amount of abrasive, temperature and impact angle on erosion morphology and rate is the significant aspect for the application and evaluation of the materials. Up to now, lots of work has been done about these aspects, respectively. The erosion morphologies and erosion rate of the WC-based coatings specimens was analyzed under the different impact angles, impact speeds, particle sizes and erosion time by Zheng *et al.* (2017), the results show these experimental parameters exerted significant effects on the erosion rates of the specimen. Li *et al.* (2020) analyzed the erosion performance of NiCr-Cr₃C₂ coatings under different impact angles, solid particle sizes and solid particle velocities, the results show the erosion rate was also improved rapidly with the increased erosion velocity for all impact angles. The effects of angle of impingement (30°, 60° or 90°) on the erosion performance of composites were evaluated by Sharma *et al.* (2017) the results show decreased angle of impingement led to reduced grain fracture and pull-out, and hence reduction in material removal. Nguyen *et al.* (2014) performed an analysis the erosion surface microstructure, erosion rate and erosion mechanism of the stainless steel at different angles, the results indicated the erosion rate at 40-degree impact angle reached the peak value; micro-cutting/plowing mechanism dominated at low impact angles while the indentation induced

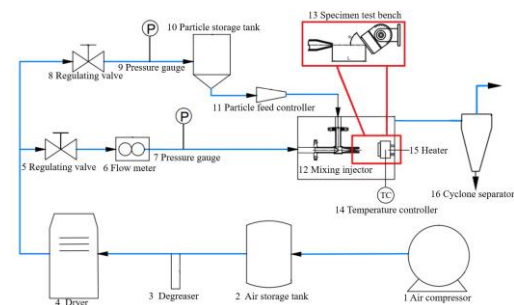
plastic deformation mechanism dominated at high impact angles.

In this paper, the experiment facility is deigned and improved based on previous study of gas-solid two-phase flow erosion wear. The material physical property of the solid particle, NiWC35 coating and sintered WC is introduced, the characterization and analysis methods of erosion rate is defined. The morphology of erosion wear and the depth of erosion pit are described and analyzed under different the amounts of abrasive, temperatures and impact angles. The microstructure of NiWC35 coating and sintered WC before and after impact was compared and explained.

2. EXPERIMENTAL PROCEDURE

2.1 Experimental Apparatus Composition

The designed experimental device flow chart is shown in Fig. 1, which is mainly divided into air supply unit, solid particle feed unit, experimental unit and exhaust gas treatment unit.



1 Air compressor 2 Air storage tank 3 Degreaser 4 Dryer 5 Regulating valve 6 Flow meter 7 Pressure gauge 8 Regulating valve 9 Pressure gauge 10 Particle storage tank 11 Particle feed controller 12 Mixing injector 13 Specimen test bench 14 Temperature controller 15 Heater 16 Cyclone separator

Fig. 1. Flow chart of gas-solid two-phase erosion test apparatus

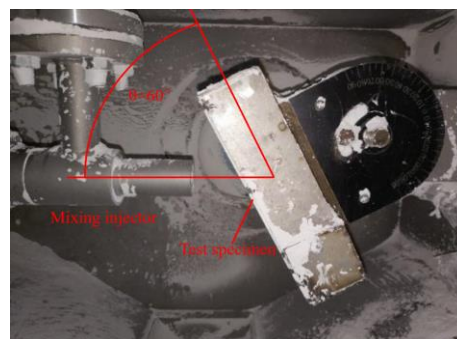


Fig. 2. Specimen test bench at 60° impact angle

Gas supply section: The air is pressurized into the air storage tank by the air compressor. Air storage tanks are used to store compressed air while

reducing the pressure pulsation due to the discontinuous compressor exhaust, achieving balance between gas supply and gas use. When the pressure of the air storage tank is stable, the valve at the outlet of the air storage tank is opened. And the high-pressure gas passes through the degreaser and the dryer in sequence, and then is supplied to the experimental part and the solid particle feed part respectively.

Solid particle feed section: The experimental solid particles were loaded into the particle storage tank and then passed through the particle feed control system to obtain the relatively constant feed rate into the experimental section.

Experimental section: The high-pressure air from the gas supply unit and the solid particles from particle storage tank were mixed in the mixing injector. Then, the test pieces on the specimen test bench were subjected to impact of the high-speed gas-solid two-phase flow, As shown in Fig. 2. The specimen test bench also contains the heater and the temperature controller to maintain the temperature of the test pieces. The impact process is carried out in the test chamber. After the test is completed, the particles enter the particle collector at the bottom of the test section for recovery.

Exhaust gas treatment section: The mixture of gas and solid particles in tail gas were separated by the cyclone separator and subsequent the bag filter.

As shown in Table 1, the experimental device of high temperature and high-speed continuous gas-solid erosion can meet the requirements for accelerating erosion wear research for abrasion resistant materials. The acceleration design of the two section of the mixing injector can make the particle velocity reach about 200m/s to impact the surface of the material, with the advantage of shortening erosion wear time. The experiment can be carried out under the temperature below 600°C.

Table 1 Specification for the erosion wear apparatus

Particle size	Particle composition	Angle of impingement	Particle speed
50~500 mesh	70% SiO ₂ , 30% Al ₂ O ₃	30~90°	200 m/s
Particle flux	Test temperature	Test pressure	Specimen size
0.05~0.5 kg/m ²	25~600 °C	0.2~0.8 MPa	65*40*10 mm ³

2.2 Material Property of Solid Particle

Sand with chemical composition of 70%SiO₂ and 30%Al₂O₃ are adopted as the material of solid particle, the density and HV hardness of sand particle is 2630kg/m³ and 1100 respectively. The microstructural morphology and general size of sand particle before the test in Fig. 3, the shape of the particle before the test is relatively irregular. The average size distribution of sand particle is about 120mesh(120µm) measured by laser particle size distribution instrument as shown in Fig. 4. The sand particles after impact are broken sharply and the edges and corners are sharper in Fig. 5.

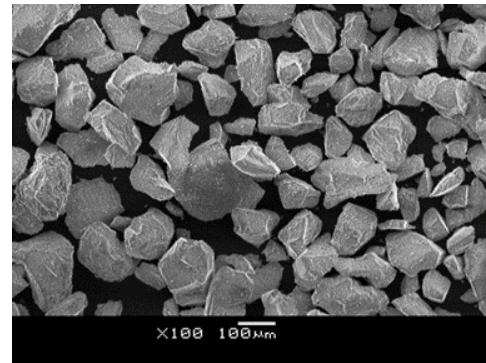


Fig. 3. Microstructural morphology of sand particle before the test

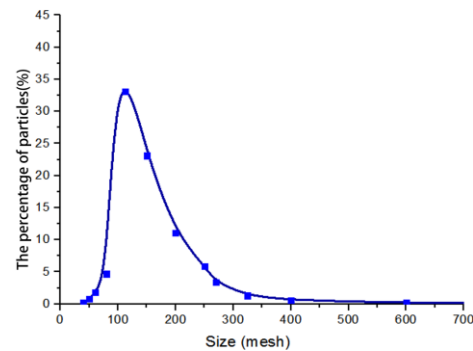


Fig. 4. Percentage distribution of sand particle size

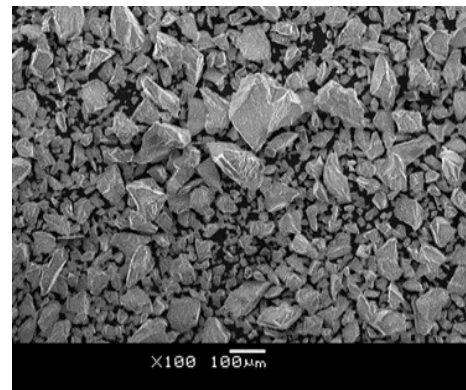


Fig. 5. Microstructural morphology of sand particle after impact

Table 2 Chemical element composition of NiWC35 coating material

	C	Cr	B	Si	Fe	W	Ni
NiWC35	2.3	10	2.5	2.9	10	28	44.3

Table 3 Parameters of NiWC35 coating material

Coating material	Substrate	Process method	size /mm ²
NiWC35	316L	PTA	40×65
Total thickness /mm	Measured net coating thickness (average) /mm	Measured coating hardness	
10	2.5,3,3.5	HRC 53~56	

2.3 Material Property of NiWC35 Coating

NiWC35 is composed of 65%Ni60 and 35% ordinary WC, which is a typical abrasion-resistant, impact-resistance spray welding material. The powdery Ni60 and WC particles are welded to the 316L stainless steel base layer by using a plasma transfer arc (PTA) process, which produces a metallurgical bond. A hard and abrasion-resistant NiWC35 coating is formed on the base layer, which has high impact-resistance. Its technology is mature and widely used in practical production, the chemical element composition of NiWC35 coating material is shown in Table 2. The size of NiWC35 coating material is 40×65mm², and its total thickness is 10mm. Its specific parameters are shown in Table 3.

2.4 Material Property of Sintered WC

WC made by integral sintering process has excellent hardness, strength, abrasion resistance and corrosion resistance, and has been widely used in cutting tools, mining tools, molds, wear parts and other fields. The WC accounts for 92% on average, Co accounts for 8%, and has good impact toughness. The size of sintered WC material is 40*65mm², and its total thickness is 10mm. Its specific parameters are shown in Table 4.

2.5 Characterization methods

Scanning electron microscopes and ultra high-speed profile measuring instrument were used to observe the surface morphology of eroded materials to investigate the mechanisms of erosion wear. In this experiment, the erosion wear rate of the material is characterized by the specimen lost mass of eroded abrasion divided by the mass of solid particles used for impacting. The relative erosion wear rate of the material is expressed as follows (Jafari *et al.*, 2014):

$$E = \frac{\Delta m_t}{m_p} \quad (1);$$

$$m_p = V_\alpha \times t \quad (2)$$

Where, E is the erosion wear rate (g/kg), Δm_t is the specimen lost mass of eroded abrasion (g), and m_p is the mass of solid particles used for impacting(kg). V_α is the impact velocity of solid particles, $V_\alpha= 9g/s$, t is experimental time.

Table 4 Sintered WC material specimen parameters

coating material	Substrate	Size/mm ²
WC (YG8)	sintered WC	40×65
Total thickness /mm	Measured net coating thickness (average) /mm	Measured coating hardness
10	10	HRC 76~77

The mass of the test specimen was measured using an electronic analytical balance. The surface of the test specimen was cleaned with an ultrasonic cleaner before and after the experiment. After drying with a hot air blower, the test specimen was measured 10 times and averaged to obtain the accurate mass before and after the test piece was subjected to erosion. The erosion pits caused by solid particle impact were observed and measured using the ultra-high-speed profile measuring instrument LK-G 5000(Fig. 6) with an accuracy of up to 0.001mm.

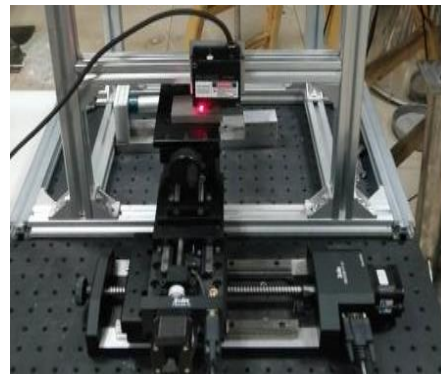


Fig. 6. Ultra high-speed profile measuring instrument

1. RESULT AND DISCUSSION

3.1 Effect of Abrasive Amount

Under the impact of different abrasive amounts, the erosion wear profile of the surface of the NiWC35 coating is shown in Fig. 7 (25°C; 90° impact angle).

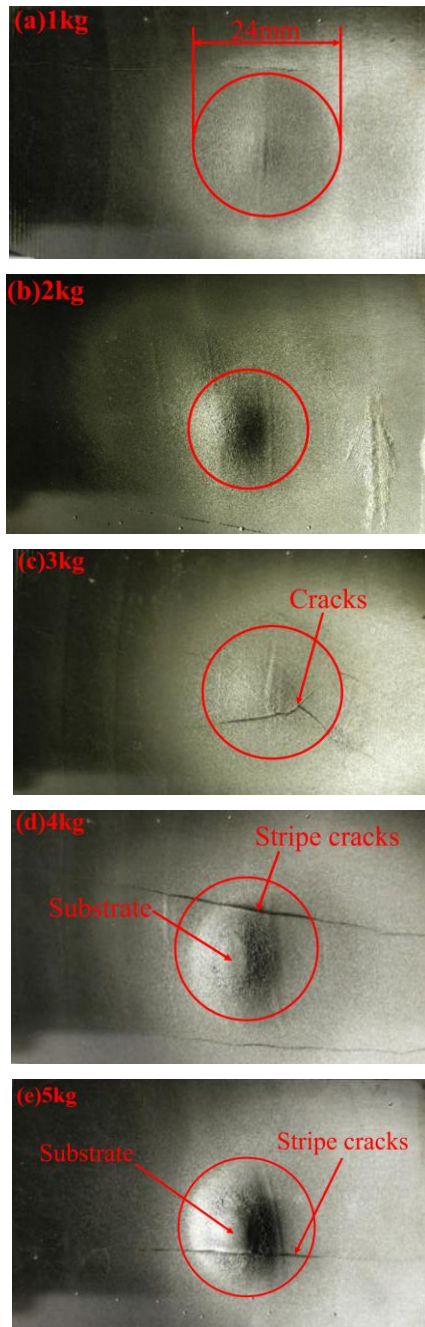


Fig. 7. Erosion wear morphology of NiWC35 coating specimens at different amounts of abrasive

It can be seen from Fig. 7 that the erosion surface of the NiWC35 coating changes significantly with the increase of the amount of abrasive. When the amount of abrasive is 1kg, the surface of the test specimen has a clear circular impact mark, the measured diameter is about 24mm, and the center has a shallowest pit; when the abrasive is added to 2kg, the impact pit is obviously deepened; when the amount of abrasive is 3kg, the depth of pit continues to deepen, and cracks appear; when the amount of abrasive is 4kg, the crack changes into stripe crack, The 316L substrate is exposed in the

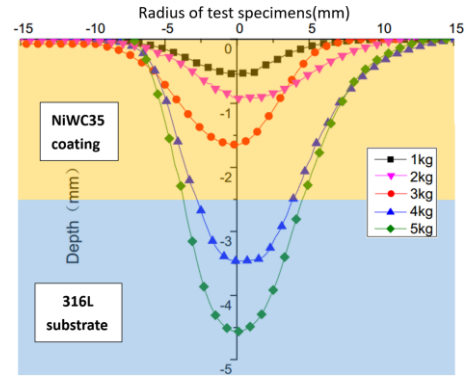


Fig. 8. Curves of erosion pit at different amounts of abrasive for NiWC35 coating specimens

deepest area of pit; when the abrasive is added to 5kg, the pit is deepest, and the NiWC35 coating on the surface is completely washed off. And it can be seen that the 316L substrate at the center of pit has been exposed. After the amount of abrasive is increased to 3kg, the NiWC35 coating will crack under the action of the impact. As cracks keep on developing, the 316L substrate is exposed and the erosion rate of 316L substrate lost to NiWC35 coating protection begins to increase significantly.

The erosion pits after the test specimens were collected using the ultra high-speed profile measuring instrument LK-G 5000. The depth-radius curves of the erosion pits were obtained as shown in Fig. 8. The depth of the NiWC35 coating specimens eroded pit increases with the increase of the abrasive amount. When the amount of abrasive is increased from 1kg to 3kg, the depth of eroded pit gradually increases by about 0.5mm/kg. when the amount of abrasive is added to 4kg, the depth of eroded pit has exceeded the thickness of the NiWC35 coating (2.5mm) and began to cause erosion wear on the 316L substrate, so change in the depth is larger than when the hard coating is eroded. From the perspective radial direction of pit, with the increase of the amount of abrasives, the erosion scope of pits is slightly increase in reason under the influence of large variation of pit depth. This also reflects from the side that the high-speed gas-solid two-phase flow emitted from the mixed injector is highly concentrated and weakly spreads outward.

From the Fig. 9(25°C; 90° impact angle), it can be seen that the eroded pit of the sintered WC is more shallow and smoother than that of the NiWC35 coating. From the surface of the test specimens, there is a marked impact imprinting ring. The diameter of the inner ring is measured to be about 20mm, the outer ring is about 26mm in the 3kg abrasive. The inner ring has an eroded concave pit obviously, while, there are lots of tiny eroded pits in the flat outer ring. This phenomenon may be due to the high speed of gas-solid impact on the surface of the test specimens, the pit depth is too shallow, the surrounding walls of the pit is not enough high to block the spread of solid particles, which will cause slight erosion damage to the outer surface of the

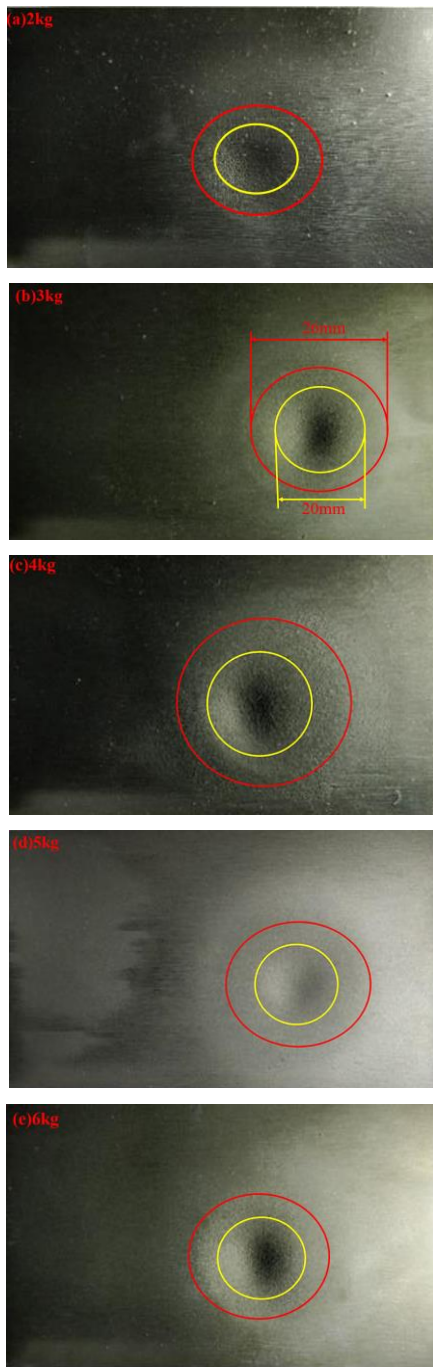


Fig. 9. Erosion wear morphology of Sintered WC specimen at different amounts of abrasive

concave pit. As the amount of abrasive increases, the depth of the concave pit changes slightly, but the change is less pronounced, showing a better resistance to grain erosion wear of the sintered WC.

It can be seen from the Fig. 10 that the depth of eroded pit of sintered WC is about 7 times as shallow as that of NiWC35 coating at the same abrasive amount. In addition, even when the amount of abrasive is added to 6kg, the depth of concave pit does not exceed 0.65mm. The radial direction range of pit is basically unchanged after the abrasive

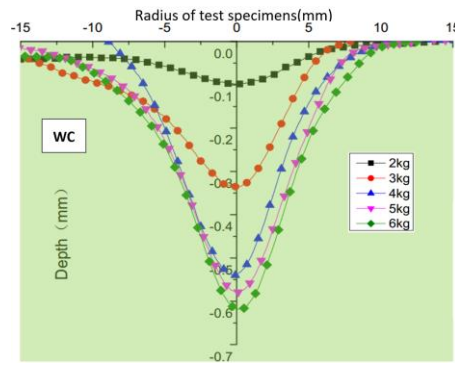


Fig. 10. Curves of erosion pits of sintered WC specimen at different amounts of abrasive

exceeds 3kg. The experimental results show that with the increase of the amount of abrasive, the depth of concave pit is extremely shallow, indicating the erosion wear resistance of the sintered WC Specimen is better.

It can be seen from Fig. 11 that the amount of abrasive has a large effect on the erosion rate of NiWC35 coating, the NiWC35 coating shows a linear growth trend when the amount of abrasive is in the 1-3kg. After the abrasive amount reaches 4-5 kg, the erosion rate of 316L substrate is higher than that of NiWC35 coating. The erosion rate of sintered WC is more less than that of NiWC35 coating material, as the amount of abrasive increases, the erosion rate does not change much.

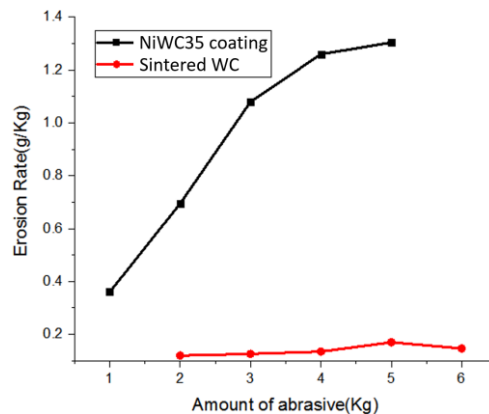


Fig. 11. Variation of erosion rate with amount of abrasive (25°C temperature; 90° impact angle)

3.2 Effect of Temperature

The erosion wear morphology of NiWC35 coating specimens at different temperatures is shown in Fig. 12(2kg abrasives; 90° impact angle). With the increase of temperature, the erosion pits deepen. After going through erosion of high temperature, the surface of NiWC35 coating appears lots of small and dense erosion pits. The small and dense erosion pits become more obvious with the rise of temperature, which also aggravate the surface roughness of the specimens. When the temperature reaches 500°C, the surface of the NiWC35 coating

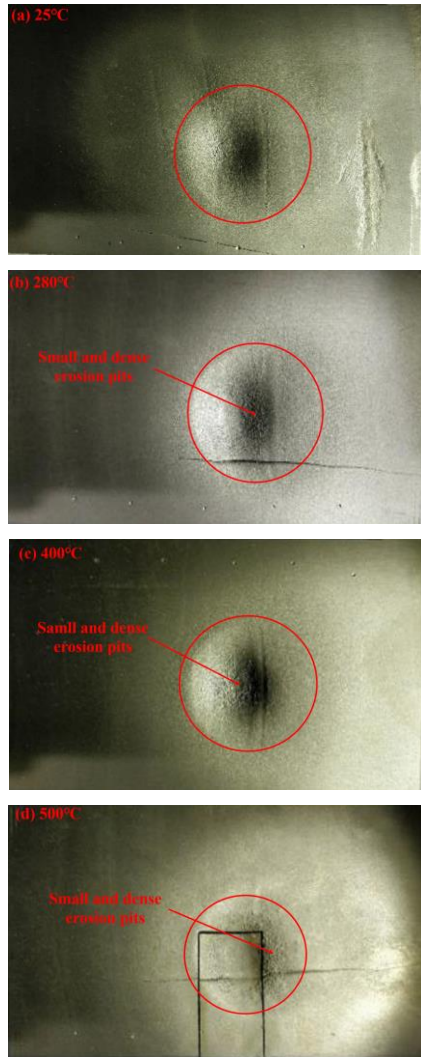


Fig. 12. Erosion wear morphology of NiWC35 coating specimens at different temperatures

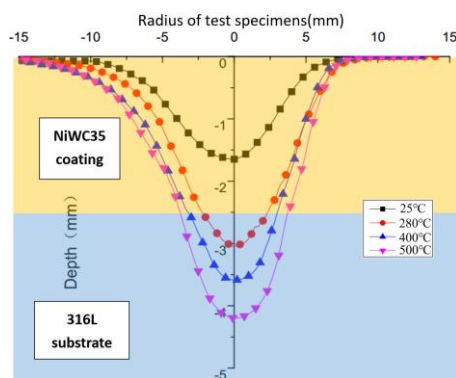


Fig. 13. Curves of erosion pits at different temperatures for NiWC35 coating

specimen has been completely washed off in the center of the pit, exposing the smooth 316L substrate. The depth-radius curves of the erosion pit is obtained by the ultra-high speed profile measuring instrument LK-G 5000, as shown in Fig.

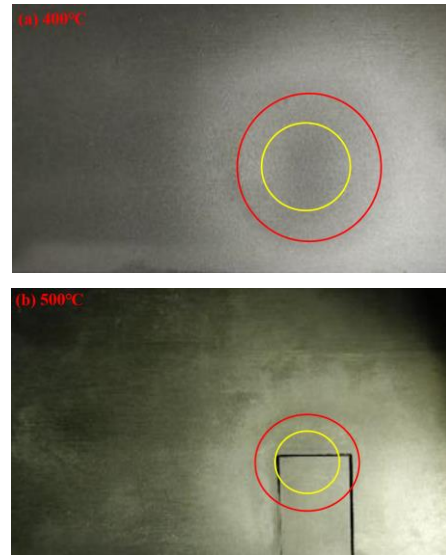


Fig. 14. Erosion wear morphology of sintered WC at different temperatures

13. With the rise of temperature, the diameter of the pit increases slightly. The depth of pit caused by 2 kg abrasive in 500°C is deeper than that of erosion by the 4kg abrasive in the 25°C. Therefore, the test temperature has a great influence on the erosion wear morphology of NiWC35 coating specimens.

The erosion characteristics of sintered WC specimens at different temperatures is comprehensively analyzed according to Fig. 14 and Fig. 15(4kg abrasives; 90° impact angle), the effect of temperature on the erosion wear topography of sintered WC is not obvious, and the surface of specimens has not significant variation, the difference of pit depth between 25°C and 500°C is less than 1mm. According to the above analysis, the abrasion resistance of sintered WC at high temperature is better than that of NiWC35 coating.

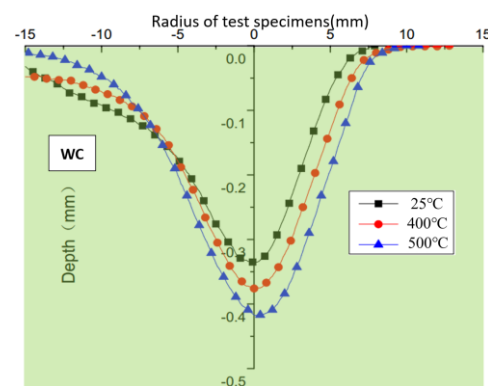


Fig. 15. Curves of erosion pits for sintered WC specimens at different temperatures

According to Fig. 11, the erosion rate of sintered WC with the same abrasive is much lower than that of NiWC35 coating. The erosion rate of sintered

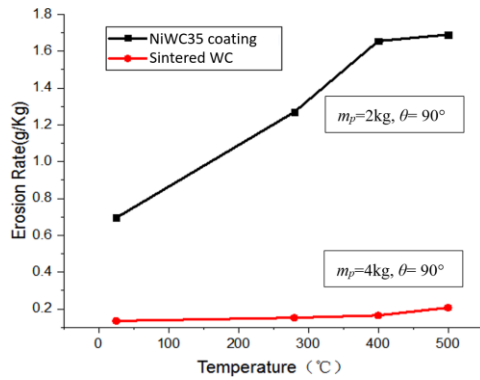


Fig. 16. Variation of erosion rate with different temperatures (Impact angle=90°)

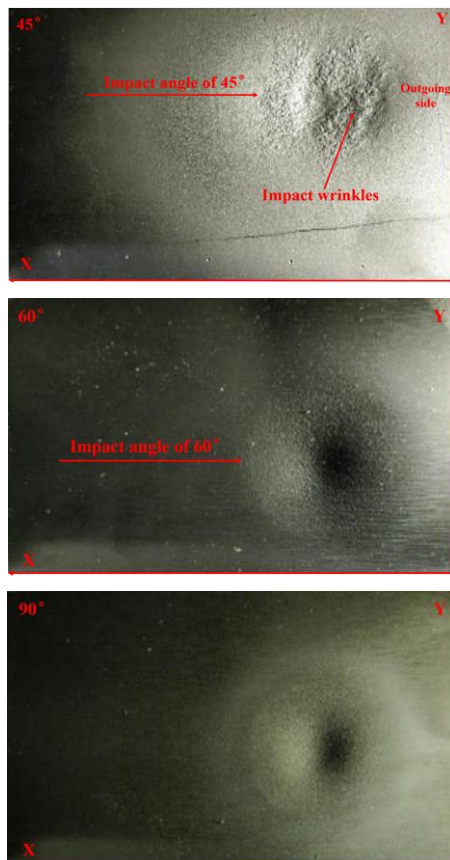


Fig. 17. Erosion wear morphology of sintered WC at different impact angles

WC with 2kg abrasive at different temperatures can not reflect the effect of temperature on sintered WC. Therefore, the erosion rate of sintered WC under 4kg abrasive was used to compare with that of NiWC35 coating under 2kg abrasive at different temperatures in Fig. 16. The erosion rate of sintered WC under 4kg abrasive also is much lower than that of NiWC35 under 2kg abrasive. The erosion rate of NiWC35 coating specimens increases linearly when the temperature is between 25- 400°C, and increases slightly between 400-500°C. The erosion rate of sintered WC is 0.131, 0.148, 0.159 and 0.203 at

25°C, 280°C, 400°C and 500°C respectively. Although the erosion rate growth value of WC sintered at 400-500°C is larger than that at other temperatures, the erosion rate of sintered WC is still much less than that of NiWC35 coating. In conclusion, the sintered WC materials have more excellent abrasive resistance than the NiWC35 coating materials at high temperature.

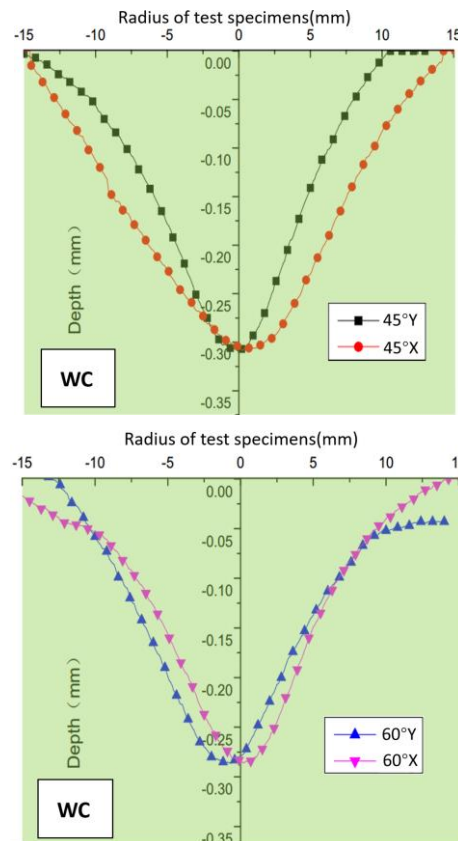


Fig. 18. Curves of erosion pits of sintered WC in different measurement directions

3.3 Effect of Impact Angle

The comprehensive analysis is made according to Fig. 17, Fig. 18 and Fig. 19(4kg abrasives; 25°C). In general, the erosion range of sintered WC varies greatly at different impact angles, and the depth of erosion pit changes little. At 45 ° impact angle, the shape of the erosion pit of sintered WC is approximately elliptical, the diameter of erosion pit in horizontal direction is larger than that in vertical direction. The surrounding surface of erosion pit is blurred due to the impact of solid particles. The erosion range at 45° impact angle is widest, the depth of erosion pit is deeper than that at the 60° impact angle and the shallower than that at the 90° impact angle. The shape of the erosion pit is approximately circular at the 60° impact angle, the erosion range is wider than that of 90° impact angle and is narrower than that at 45° impact angle. At the 90° impact angle, the erosion range is narrowest and the depth of pit is the deepest.

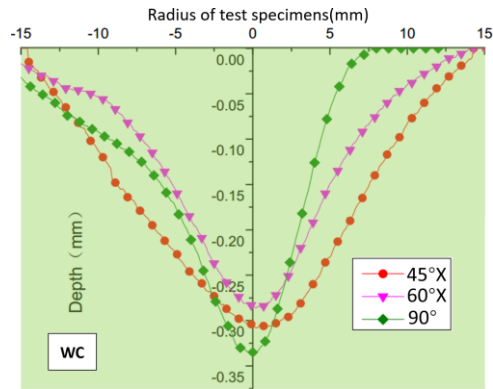


Fig. 19. Curves of erosion pits for sintered WC at different impact angles

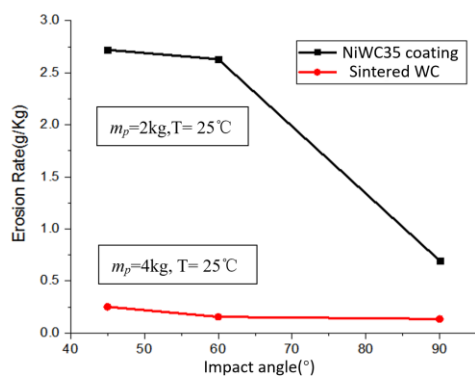


Fig. 20. Variation of erosion rate at different impact angles

The erosion rate at different impact angles is shown in Fig. 20. The erosion rate of NiWC35 coating material at 45° impact angle is slightly higher than that at 60° impact angle, and the erosion rate at 90° impact angle is the minimum, which is only 0.27 times of that at 45° impact angle. The erosion rate of sintered WC materials has little difference at different impact angles. All in all, the erosion rate of sintered WC materials is much lower than that of NiWC35 coating materials at the different impact angles.

3.4 The Micromorphology Analysis

Scanning the test specimens by electron microscopy can get the combined appearance of the NiWC35 coating and the 316L substrate before the experiment as shown in Fig. 21, where (a), (b) are enlarged image of 100 times and 200 times respectively. The scans clearly show the obvious difference between the NiWC35 coating and the 316L substrate. In the (a), there are many protruding white NiWC35 particles on the surface of NiWC35 coating on the left of image, while the 316L substrate is relatively flat and smooth on the right of image, it is difficult to resist the erosion of solid particles, compared with NiWC35 coating. The 200 times enlarged image of NiWC35 coating can be clearly seen from (b). There are some small pits on the surface of NiWC35 coating, which leads to the

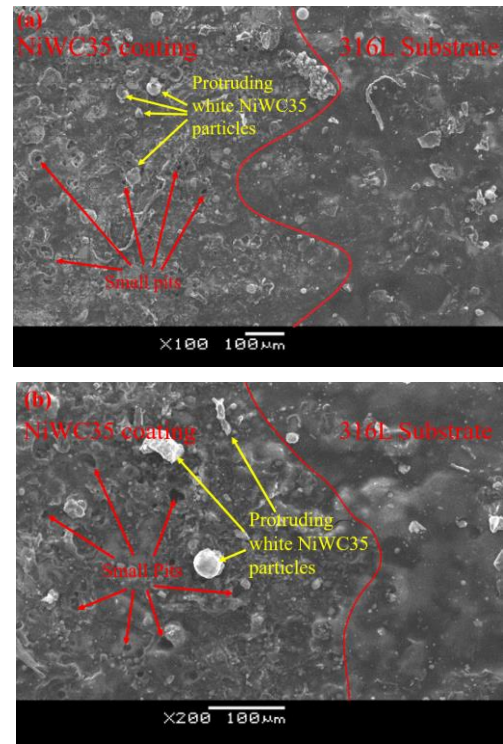


Fig. 21. Micromorphology of NiWC35 coating specimens

surface is not compact enough to resist the erosion of solid particles.

As shown in Fig. 22, where (a) is the interface between the NiWC35 coating and the 316L substrate when the erosion pit is just eroded to the substrate. The surface of the 316L substrate in the lower left corner is relatively smooth and flat, while the NiWC35 coating in the upper right corner shows many protruding white NiWC35 particles embedded in the substrate. It can be seen from (b) that these protruding white NiWC35 particles are approximately spherical, the adhesive around them has been washed away and these white NiWC35 particles bulged to resist the impact of the abrasive. (c) and (d) are the morphology of the protruding NiWC35 spherical particles at a magnification of 1000 times. when the bonding matrix around the NiWC35 spherical particles is eroded too much, the integrated NiWC35 spherical particle is exposed as shown in the (c). At the same time, when the bonding matrix around NiWC35 spherical particles is still firm, the protruding portion of NiWC35 spherical particles is directly broken as shown in the (d), so it can be seen that the hardness of the NiWC35 spherical particle is not high. The diameter of the NiWC35 spherical particle is measured to be about 80μm, which is too coarse compared to the size of the countless irregular particle of the sintered WC in Fig. 23 below. From the above analysis, it can be seen that the NiWC35 coating has the defects of high porosity, the coarse and loose of NiWC35 spherical particles, which also results in easy erosion damage of NiWC35 coating surface.

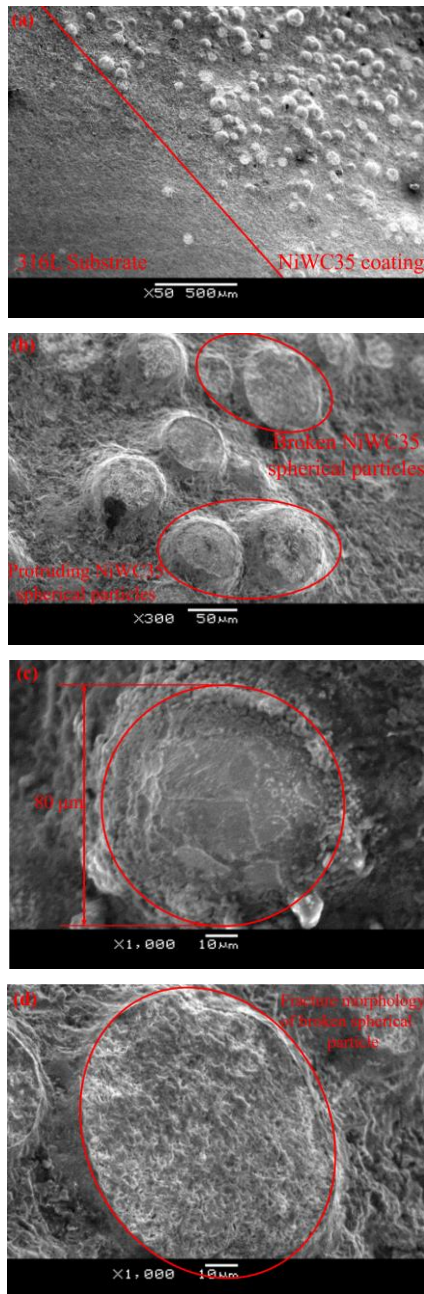


Fig. 22. Micromorphology of NiWC35 coating specimen

The photomicrograph of sintered WC surface obtained by scanning electron microscopy is shown in Fig. 23, in which (a) and (c) are electron microscopy scan image of 1000 and 2000 magnifications of the uneroded surface topography, while (b) and (d) are electron microscopy scan images of 1000 and 2000 magnification of the eroded surface topography, respectively. The microstructure of the sintered WC material is bound together by countless irregular particles of The size of the particles is about 1-5 μ m, which is small and compact compared to the surface of NiWC35 coating, so that abrasion resistance of sintered WC is greatly improved. By comparing the surface morphology before and after impact in Fig. 23, the

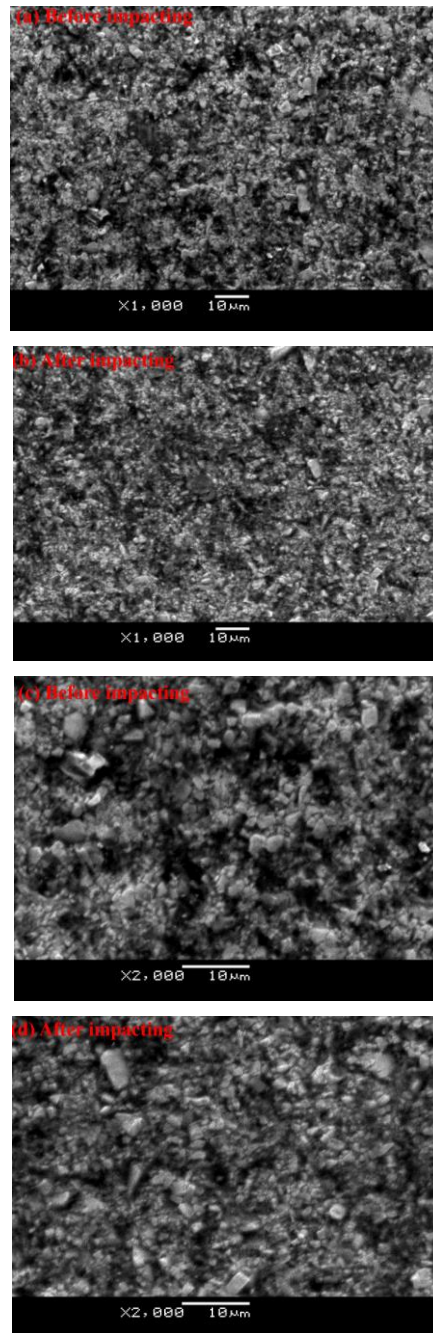


Fig. 23. Compared micromorphology of sintered WC before and after impacting.

surface of sintered WC after impacting has smaller gaps, becoming more compact than the before of impacting. The gap is even smaller than size of the impact solid particles. Compared with previous analysis of NiWC35 coating, there is no phenomenon that the adhesive is washed away. Therefore, it can be seen that the compact countless irregular particles are the key to the great abrasion resistance of sintered WC.

2. CONCLUSION

In this paper, the experimental facility self-designed of high temperature, different impact angles and high-speed continuous gas-solid erosion is set up,

which can meet the requirements of accelerating erosion wear research process for abrasion resistant materials. The macroscopic and microscopic erosion morphology and erosion rate of NiWC35 coating and sintered WC were analyzed and discussed.

1. The erosion rate of NiWC35 coating increases approximately linearly with the increase of the amount of abrasive, which is more greater than the erosion rate of the sintered WC; the erosion rate of the NiWC35 coating obviously increase with the rise of temperature; the impact angle of the NiWC35 coating is smaller, the range of erosion pit is wider, the wrinkles in outgoing side caused by solid particles is more, the erosion rate is larger.

2. The sintered WC have excellent abrasive resistance, the erosion wear morphology and erosion rate basically unchanged under different amounts of abrasive, different temperatures, and different impact angles.

3. The diameter of protruding NiWC35 spherical particles is measured to be about 80 μ m, which is too coarse compared to the size of the irregular particle of the sintered WC. During the impact process, the adhesive around NiWC35 spherical particles has been washed away, the NiWC35 spherical particles are exposed, detached and broken, and the surface of NiWC35 coating are easily cracked. While the gaps of countless irregular particles in the sintered WC material are less than that of before impacting, the diameter of these particles is about 1-5 μ m, it is key to the excellent abrasion resistance of sintered WC.

ACKNOWLEDGEMENTS

The authors acknowledge the financial support provided by the National Key R&D Project of China (2018YFB2004002) and Zhejiang Provincial Natural Science Foundation of China (LY21E060011).

REFERENCES

- Bhosale, D. G., T. R. Prabhub and W. S. Rathod (2020). Sliding and erosion wear behavior of thermal sprayed WC-Cr₃C₂-Ni coatings. *Surface & Coatings Technology* 400, 126192.
- Chen, M., H. Lu., Y. Jing., X. Guo, X. Gong and H. Liu (2020). Experimental and numerical study on gas-solid two-phase flow through regulating valve of pulverized coal flow. *Chemical Engineering Research and Design* 155, 1-11.
- Hu, K. and S. J. Kim (2020). Effect of various factors on solid particle erosion behavior of degraded 9Cr-1MoVNb steel with experiment design. *Applied Surface Science* 506, 144956.
- Ilieva, G (2017). Mechanisms of water droplets deposition on turbine blade surfaces and erosion Wear Effects. *Journal of Applied Fluid Mechanics* 10(2), 551-567.
- Jafari, M., Z. Mansoori, M. S. Avval, G. Ahmadi and A. Ebadi (2014). Modeling and numerical investigation of erosion rate for turbulent two-phase gas-solid flow in horizontal pipes. *Powder Technology* 267, 362-370.
- Kim, J. H., H. G. Joo and K. Y. Lee (2015). Simulation of solid particle erosion in WC-Ni coated wall using CFD. *Journal of Materials Processing Technology* 224, 240-245.
- Kumar, H., C. Chittosiya and V. N. Shukla (2018). HVOF sprayed WC based cermet coating for mitigation of cavitation, erosion & abrasion in hydro turbine blade. *Materials Today: Proceedings* 5, 6413-6420.
- Li, Y. and C. Li (2019). Fossil energy subsidies in china's modern coal chemical industry. *Energy Policy* 135, 111015.
- Li, Z., Y. Li, J. Li, F. Li, H. Lu, J. Du, X. Ran and X. Zhang (2020). Effect of NiCr content on the solid particle erosion behavior of NiCr-Cr₃C₂ coatings deposited by atmospheric plasma spraying. *Surface & Coatings Technology* 381, 125144.
- Lin, Z., X. Sun, T. Yu, Y. Zhang, Y. Li and Z. Zhu (2020). Gas-solid two-phase flow and erosion calculation of gate valve based on the CFD-DEM model. *Powder Technology* 366, 395-407.
- More, S. R., D. V. Bhatt and J. V. Menghan (2018). Failure analysis of coal bottom ash slurry pipeline in thermal power plant, *Engineering Failure Analysis* 90, 489-496.
- Nguyen, Q. B., V. B. Nguyen and C. Y. H. Lim (2014). Effect of angle of impingement and testing time on erosion of stainless steel at higher velocities. *Wear* 321, 87-93.
- Ou, G., P. Ouyang, Z. Zheng, H. Jin, K. Bie and C. Wang (2019). Investigation on failure process and structural improvement of a high-pressure coal water slurry valve. *Engineering Failure Analysis* 96, 1-17.
- Sharma, S. K., B. V. M. Kumar and Y. W. Kim (2017). Effect of impingement angle and WC content on high temperature erosion behavior of SiC-WC composites. *International Journal of Refractory Metals & Hard Materials* 68, 166-171.
- Singh, V., S. Kumar and S. K. Mohapatra (2019). Modeling of erosion wear of sand water slurry flow through pipe bend using CFD. *Journal of Applied Fluid Mechanics* 12(3), 679-687.
- Varga, M., M. Antonov, M. Tumma, K. Adam and K. O. Alessioci (2019). Solid particle erosion of refractories: A critical discussion of two test standards. *Wear* 426-427, 552-561.
- Xiao, J., S. Wang., S. Ye., J. Dong., J. Wen and Z. Zhang (2020). Thermo-economic optimization of gasification process with coal water slurry preheating technology. *Energy* 199, 117354.
- Zheng, C., Y. Liu, J. Qin, W. Ji, S. Zhang, R. Ji and B. Cai (2017). Experimental study on the erosion behavior of WC-based high-velocity

C. Wang *et al.* / *JAFM*, Vol. 14, No. 4, pp. 1125-1136, 2021.

oxygen-fuel spray coating. *Powder Technology* 318, 383–389.

Zheng, Z., G. Ou, Y. Yi, G. Shu, H. Jin, C. Wang and H. Ye (2016). A combined numerical-

experiment investigation on the failure of a pressure relief valve in coal liquefaction. *Engineering Failure Analysis* 60, 236-340.